

Self-Radiography of Imploded Shells on OMEGA Based on Additive-Free Multi-Monochromatic Continuum Spectral Analysis

R. Epstein,¹ R. C. Mancini,² D. T. Cliche,² R. C. Shah,¹ T. J. B. Collins,¹ C. Stoeckl,¹ P. W. McKenty,¹ P. B. Radha,¹
S. P. Regan,¹ and V. N. Goncharov¹

¹Laboratory for Laser Energetics, University of Rochester

²University of Nevada, Reno

Cryogenic implosions on the OMEGA Laser System¹ can be self-radiographed by their own core spectral emission near ≈ 2 keV. Utilizing the distinct spectral dependences of continuum emissivity and opacity, the projected optical thickness distribution of imploded shells can be distinguished from the structure of the core emission in images. This can be done without relying on spectral additives (shell dopants), as in previous applications of implosion self-radiography.² Demonstrations with simulated data show that this technique is remarkably well-suited to cryogenic implosions. Imploded room-temperature CH shells can also be self-radiographed at higher spectral energy ($h\nu \approx 3$ to 5 keV) based on the very similar continuum spectrum of carbon. Experimental demonstration of additive-free self-radiography with warm CH shell implosions on OMEGA will provide an important proof of principle for future applications to cryogenic DT implosions.

Externally backlit radiography³ is primarily sensitive to the shape of the limb of the shell as projected onto an image plane and requires spectral filtering and/or temporal gating techniques⁴ to keep the core from outshining the external backlighter as the implosion approaches peak conditions. Self-radiography sidesteps this limitation by using core self-emission as the backlighter to project the structure of the near face of the shell onto an image plane.

We formulate continuum radiography as a spectral analysis of the imaged intensity at each image pixel, based on the free-free and bound-free emissivity and opacity of hydrogen-like ions as described by the Kramer's⁵ semi-classical expressions with power-law Gaunt factor corrections^{6,7} based on Karzas and Latter,⁸ of the form $g_\nu \propto (\nu/\nu_0)^{-q}$. For the anticipated spectral range for CH shell implosions, $3.6 < h\nu_0 < 5.4$ keV, the likely index value at the spectral midpoint is $q \approx 0.11$. The index rises slowly to $q \approx 0.5$ in the limit that the spectral energy greatly exceeds the electron binding energy, which applies to hydrogen.

The shell optical thickness at a nominal spectral frequency ν_0 can be expressed in terms of the power law $\tau_\nu \propto (\nu/\nu_0)^{-(3+q)}$. In local thermodynamic equilibrium, the emissivity spectral form is obtained from the opacity by the Kirchhoff relationship⁹ using the Planck function. The result is a phenomenological expression of the intensity spectrum for a thermal continuum emitter surrounded by a non-emitting layer

$$I_\nu = A(\nu_0/\nu)^q e^{-(1-\nu/\nu_0)/t - \tau_0(\nu_0/\nu)^{3+q}}, \quad (1)$$

where A represents the unabsorbed emission, τ_0 is the optical thickness of the foreground absorber, and $t = kT/h\nu_0$ is a local continuum slope parameter that can be interpreted as an emission-weighted, harmonic mean of the source electron temperature. These three parameters are estimated at each pixel.

The three spectral parameter estimates will be sensitive to signal noise. With three images covering a bandwidth $\Delta\nu$ and with pixel intensities precise to a standard deviation equal to a fraction σ_I , the resulting formal uncertainty of the τ estimates, for example, in the small- $\Delta\nu$ limit is $\delta\tau \cong \sqrt{2/3} \sigma_I (\nu_0/\Delta\nu)^2$. It is clear from the strong $\Delta\nu$ scaling of this expression that broad bandwidth is essential.

We apply our proposed analysis to synthetic data based on radiation-hydrodynamic simulations to show that the emission and absorption separation expressed in Eq. (1) is valid and that radiographs can be successfully inferred. The example selected here is based on a 2-D *DRACO*¹⁰ simulation of the implosion experiment shot 81590 (Ref. 4). Figure 1 shows three simulated images at spectral energies $h\nu = 1.6, 1.8,$ and 2.0 keV, obtained from this simulation at a time near peak neutron production with the radiation-transport postprocessor *Spect3D*.¹¹ The view direction is 30° above the equatorial plane. The *DRACO* simulation includes the effects of nonuniform laser irradiation, including the ideal single-beam intensity profile, OMEGA's 60-beam pattern, and fine-scale beam speckle. The image structure in any one image is the net result of emission followed by absorption. Separating the absorption structure from the emission structure by spectral analysis is the basis of self-radiography.

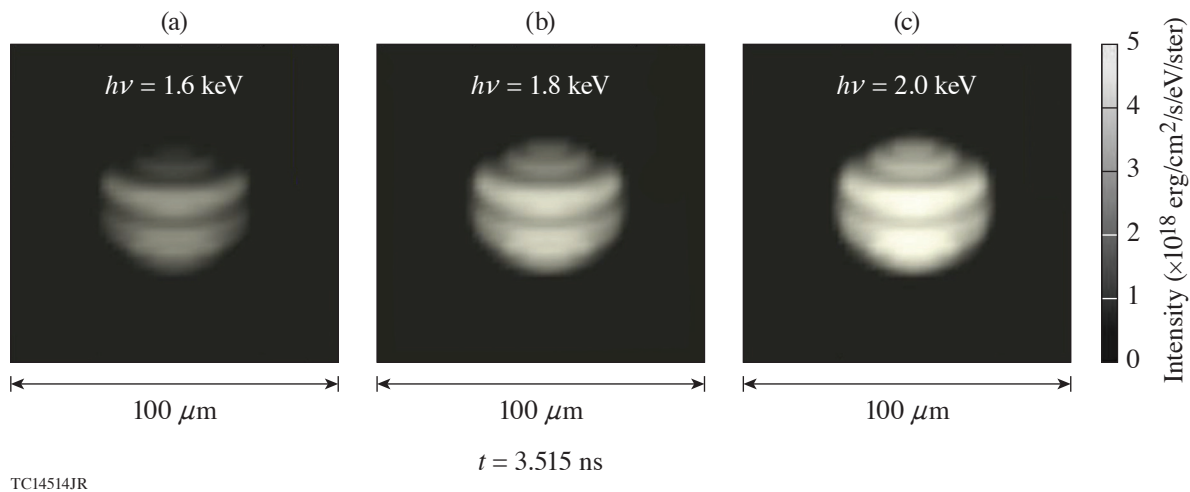


Figure 1

Three simulated monochromatic images of the OMEGA implosion experiment shot 81590 at spectral energies (a) $h\nu = 1.6$, (b) 1.8 , and (c) 2.0 keV at a time near peak neutron production.

Pixel-by-pixel spectral analysis based on Eq. (1) produces the unabsorbed emission distribution shown in Fig. 2(a) and the radiograph in Fig. 2(b), both at $h\nu = 1.8$ keV. The radiograph shows the optical thickness increasing from just below unity at the center to about double that at the edge. This absorption profile changes the roughly uniform appearance of the bare emission distribution in Fig. 2(a) into the centrally bright appearance of the simulated images in Fig. 1.

The radiograph in Fig. 2(b) is most useful within a circular area whose diameter is approximately the length of the red spatial reference arrow. The analysis produces optical thicknesses further out from the center, but this is beyond the outer edge of the emitting core, where the fitting model may be misapplied and where the image signal may be too weak to use, relative to instrumental noise, etc. To show that the radiograph is quantitative where the image signal is reasonably strong, we compare the inferred optical thickness at 20 points on the image plane along the spatial reference arrow with the optical thickness calculated directly from the image simulation model. These are shown as the “inferred” and “actual” points in the plot in Fig. 2(c), respectively. The agreement is very good. The inferred values are all slightly lower than the actual values because a small part of the actual total optical thickness exists in the emitting core where it is only partially effective in attenuating the core emission.

We anticipate a proof-of-principle demonstration of continuum-based self-radiography of OMEGA implosions using imploded CH polymer shells imaged with the multiframe monochromatic imager (MMI) instrument.¹² The MMI combines Bragg reflection with a pinhole array to provide time-gated images of inertial confinement fusion implosions. The quantitative capabilities of the MMI have been most recently characterized quantitatively by Cliche *et al.*¹³ The current configuration operates with a broad 3.5- to 5.5-keV spectral range and independent electro-optic time gating along four strips on a multichannel photoelectron-multiplying detector plate at the image plane. The MMI could be also be used for self-radiography of cryogenic implosions at lower spectral

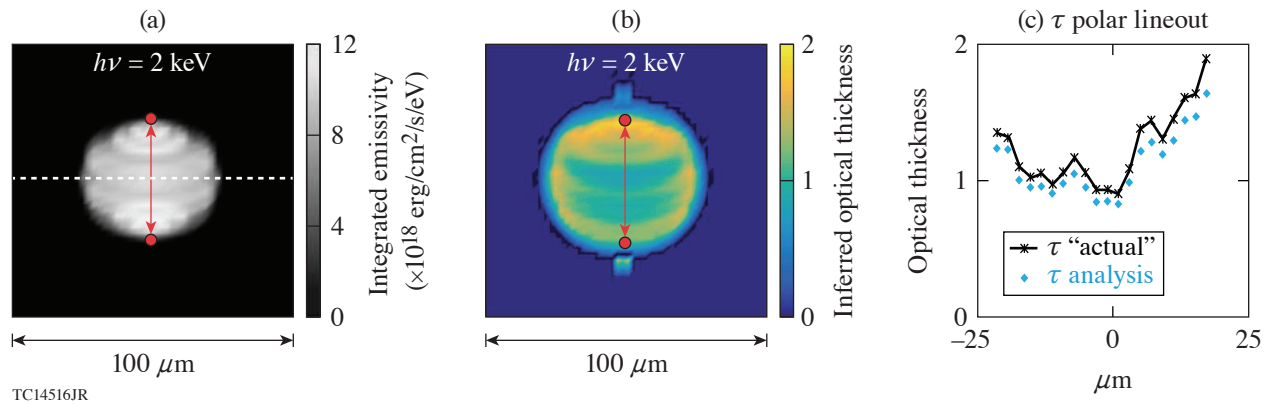


Figure 2

Analysis results showing the (a) unabsorbed emission distribution, (b) inferred radiograph, and (c) a vertical lineout of the radiograph optical thickness showing agreement between inferred and simulated “actual” optical thickness. (a) and (b) represent the spectral energy $h\nu = 1.8$ keV.

ranges near $h\nu \approx 2$ keV. A theoretical basis for analyzing MMI images of continuum emission in terms of an ideal spherically symmetric source model has already been described.¹⁴ Successful self-radiography of room-temperature CH implosions would be an important and encouraging prelude to continuum-based self-radiography of cryogenic DT shell implosions.

This material is based upon work supported by the Department of Energy National Nuclear Security Administration under Award Number DE-NA0003856, the University of Rochester, and the New York State Energy Research and Development Authority.

1. T. R. Boehly *et al.*, *Opt. Commun.* **133**, 495 (1997).
2. V. A. Smalyuk *et al.*, *Phys. Rev. Lett.* **87**, 155002 (2001); L. A. Pickworth *et al.*, *Phys. Rev. Lett.* **117**, 035001 (2016).
3. R. Epstein *et al.*, *High Energy Density Phys.* **23**, 167 (2017).
4. C. Stoeckl *et al.*, *Phys. Plasmas* **24**, 056304 (2017).
5. H. A. Kramers, *Philos. Mag.* **46**, 836 (1923).
6. J. A. Gaunt, *Proc. R. Soc. Lond. A* **126**, 654 (1930).
7. H. R. Griem, *Principles of Plasma Spectroscopy* (Cambridge University Press, Cambridge, England, 1997).
8. W. J. Karzas and R. Latter, *Astrophys. J. Suppl. Ser.* **6**, 167 (1961).
9. S. Chandrasekhar, *Radiative Transfer* (Dover Publications, New York, 1960).
10. P. B. Radha *et al.*, *Phys. Plasmas* **12**, 032702 (2005); J. A. Marozas *et al.*, *Phys. Plasmas* **25**, 056314 (2018).
11. J. J. MacFarlane *et al.*, *High Energy Density Phys.* **3**, 181 (2007); Prism Computational Sciences Inc., Madison, WI 53711.
12. J. A. Koch *et al.*, *Rev. Sci. Instrum.* **76**, 073708 (2005).
13. D. T. Cliche and R. C. Mancini, *Appl. Opt.* **58**, 4753 (2019).
14. J. A. Koch, S. W. Haan, and R. C. Mancini, *J. Quant. Spectrosc. Radiat. Transf.* **88**, 433 (2004).